Diagn Interv Radiol DOI 10.5152/dir.2019.18337

HEAD AND NECK IMAGING

ORIGINAL ARTICLE

Basal cell adenoma and myoepithelioma of the parotid gland: patterns of enhancement at two-phase CT in comparison with Warthin tumor

Ji Young Lee
Hyung-Jin Kim
Yi Kyung Kim
Jihoon Cha
Sung Tae Kim

PURPOSE
Early enhancement and a washout pattern are reported to be the characteristic imaging features of Warthin tumor (WT). The purpose of this study was to evaluate the enhancement patterns of basal cell adenoma (BCA) and myoepithelioma (ME) of the parotid gland on two-phase computed tomography (CT), compared with WT.

METHODS
We retrospectively evaluated two-phase CT examinations of histologically proven 19 BCAs, 12 MEs, and 23 WTs of the parotid gland. In all patients, CT scans were obtained at early and delayed phases with scanning delays of 40 and 180 s, respectively. We measured the attenuation values on each phase of CT scans and calculated washout attenuation and relative percentage enhancement washout ratio. From the data acquired, we statistically compared the enhancing characteristics among three tumor groups.

RESULTS
Based on the results of washout attenuation and relative percentage enhancement washout ratio, 15 (79%) of 19 BCAs, 9 (75%) of 12 MEs, and 23 (100%) of 23 WTs demonstrated a washout pattern of enhancement on two-phase CT scans. Despite variations of the individual tumors, both parameters revealed no significant difference among three tumor groups.

CONCLUSION
BCAs and MEs of the parotid gland frequently show early enhancement and a washout pattern on two-phase CT, which can be indistinguishable from WTs in the majority of cases.

Parotid tumors account for about 3% of all head and neck tumors. Of parotid tumors, 80%–85% are benign, most of which are pleomorphic adenoma (PA) and Warthin tumor (WT) (1). The preoperative imaging examinations of parotid tumors are important for differentiation between benign and malignant tumors as well as localization of intraparotid facial nerve and include ultrasonography, computed tomography (CT), and magnetic resonance imaging (MRI) (2–12). However, the efficacy of preoperative imaging is still controversial for differentiating the tumors of various histologic types because of wide range of overlap between the imaging findings.

Two-phase CT is an abbreviated form of dynamic contrast-enhanced CT technique, which can provide functional analysis through the essential information on perfusion of the lesion (2, 13). As described by Choi et al. (2), this technique is well known for differentiation of WTs from other tumors of the parotid gland, including PAs and malignant tumors. They reported early enhancement and washout of contrast material as the characteristic enhancement pattern of WTs. Using immunohistochemical staining, Woo et al. (13) showed that abundant blood vessels and extensive capillary networks as well as lack of complete vessel wall coverage form the pathologic basis for the enhancement pattern of WTs at two-phase CT. They also reported significantly different enhancement pattern in WTs compared with a group of benign tumors other than PAs.

In our experience, basal cell adenomas (BCAs) and myoepitheliomas (MEs), both of which are unusual benign tumors of the salivary gland, frequently demonstrate an enhancement

From the Department of Radiology (J.Y.L.), Hanyang University Hospital, Hanyang University School of Medicine, Seoul, Korea; Department of Radiology (H.J.K. ✉ *hyungkim@skku.edu*, Y.K.K., S.T.K.), Samsung Medical Center, Sungkyunkwan University School of Medicine, Seoul, Korea; Department of Radiology (J.C.), Research Institute of Radiological Science, Yonsei University School of Medicine, Seoul, Korea.

Received 23 July 2018; accepted 21 October 2018.

Published online 23 May 2019.

DOI 10.5152/dir.2019.18337

You may cite this article as: Lee JY, Kim HJ, Kim YK, Cha J, Kim ST. Basal cell adenoma and myoepithelioma of the parotid gland: patterns of enhancement at two-phase CT in comparison with Warthin tumor. Diagn Interv Radiol 2019; DOI 10.5152/dir.2019.18337.

pattern similar to WTs at two-phase CT scanning. Although several studies have reported the general imaging features of BCAs (14–17) and MEs (18, 19), only a few have dealt with their enhancement pattern on dynamic CT and MRI examinations including two-phase CT (16, 20–22). Furthermore, to our knowledge, there have been no comparative studies on the enhancement pattern between these tumors and WTs on two-phase CT. The purpose of this study was to investigate the differences, if any, in the enhancement pattern among BCAs, MEs, and WTs on two-phase CT.

Methods

Study subjects

Our study was approved by our institutional review board (IRB file no. SMC 2018-07-127) and informed consent was waived in accordance with the requirements of a retrospective study. Between 2005 and 2014, a search of medical records from an electronic database in our institution identified 26 patients with BCA and 15 patients with MEs of the parotid gland. After exclusion for absence of two-phase CT scanning, we included 19 patients (5 men, 14 women; mean age, 62 years; range, 39–75 years) with BCA and 10 patients (3 men, 7 women; mean age, 56 years; range, 21–74 years) with ME. All patients with BCA and 8 of 10 patients with ME had single lesion, while two patients with ME, both of whom had a history of previous surgery, had two lesions on the same side of the operated parotid gland. For controls, consecutive 20 patients (19 men, 1 woman; mean age, 55 years; range, 47–71 years) with WT who underwent two-phase CT examination in 2013 were collected from the database of the Radiology Department of our hospital. Three of the 20 patients with WT had two lesions on the same side (n=1) or on both sides (n=2) of the parotid gland. Finally, we included 19 BCAs, 12 MEs, and 23 WTs, which formed the basis of this study. The diagnosis was confirmed histologically by surgery in all lesions including multiple tumors in patients with ME and WT.

Main points

- Warthin tumors are well-known for the characteristic washout of contrast material at two-phase CT scanning, an abbreviated form of dynamic contrast-enhanced CT technique that can provide functional analysis through the essential information on perfusion of the lesion.
- Although rare, basal cell adenomas and myoepitheliomas also often demonstrate an enhancement pattern that is hard to differentiate from that of Warthin tumors at two-phase CT.
- The washout pattern of enhancement seen in these tumors seems to reflect the prominent vasculature within the solid component of the tumors histologically.

CT scanning and analysis

For all patients, two-phase CT scans were obtained in the axial plane from thoracic inlet to inferior orbital ridge by using various models of a multidetector-row CT scanner with 2.5 to 3.75 mm section thickness. After the intravenous administration of 90 mL of iodinated contrast material into an antecubital vein at a rate of 3 mL/s with a power injector, early and delayed phase scans were obtained with scanning delays of 40 and 180 s, respectively. Based on the dose report generated by CT scanner, mean volumetric CT dose index (CTDIvol) was 28.2 mGy per phase of CT scanning (range, 10.9–37.5 mGy) and mean dose-length product (DLP) was 792 mGy·cm (range, 206–1559 mGy·cm).

CT scans were interpreted by a dedicated head and neck neuroradiologist and a general neuroradiologist in consensus, who have been practicing in the field for 26 years and 5 years, respectively. They were blinded to the pathology results. First, we recorded the general morphologic characteristics of the tumor, such as the size (at its greatest diameter), location (superficial or deep lobe), margin (well-defined, microlobulated, or indistinct), and presence of the cystic change or calcification. Second, for quantitative analysis of the enhancing characteristics, we measured CT attenuation values (in HU) on early (40 s) and delayed (180 s) CT scans by placing the largest possible circular region of interest (2.6–124.5 mm^2) within the solid portion of the lesion with caution to avoid the cystic area. From these, as described by Kamiyama et al. (23), we calculated the following diagnostic parameters in each tumor: washout attenuation (A_{WO}) as $A_{WO} = A_E - A_D$, where A_E is attenuation value on early-phase CT scan and A_D is attenuation value on delayed-phase CT scan; and relative percentage enhancement washout ratio (RPEWR) as RPEWR (%) = $(A_{WO} / A_E) \times 100$. From the data acquired, we compared the enhancing characteristics on two-phase CT between each tumor group. We defined the washout enhancement pattern as $A_E > A_D$. When $A_E < A_D$, it was defined as the gradual enhancement pattern.

Statistical analysis

The general morphologic features among three groups of tumor were compared using Fisher exact test. The differences in mean ± SD values of tumor size, A_E, A_D, A_{WO}, and RPEWR among three tumor groups were statistically evaluated by the analysis of variance test with the Tukey test as a post hoc test. Statistical analysis was performed by using the PASW software version 18.0 (SPSS Inc.) and $P < 0.05$ was considered statistically significant.

Results

The general morphologic characteristics of the three different tumor groups are summarized in Table 1. No statistically significant differences were found among the three tumor groups with regard to the size, location, margin, cystic change, and calcification. Among 19 BCAs, 12 MEs, and 23 WTs, the mean size of the tumors was greatest for WT (2.8±0.89 cm), followed by BCA (2.4±1.15 cm) and ME (2.3±0.86 cm). The superficial lobe was the predominant location of all three tumors: 15 BCAs (78.9%), 10 MEs (83.3%), and 18 WTs (78.3%) were located in the superficial lobe. Most tumors had a well-defined margin, seen in 18 BCAs (94.7%), 11 MEs (66.7%), and 22 WTs (95.7%). The cystic change was demonstrated in 9 BCAs (47.4%), 6 MEs (50%), and 7 WTs (30.4%). Calcification was infrequent for all three tumors, seen in two BCAs (10.5%), one ME (8.3%), and one WT (4.3%).

Results of the various CT parameters for the three tumors and their statistical comparisons are summarized in Tables 2 and 3. ME showed greater mean values for both A_E (141.0±38.4) and A_D (101.7±18.2) than BCA (114.6±39.3 and 83.5±24.6, respectively) and WT (103.4±20.2 and 70.2±11.8, respectively). Statistically significant difference was found between ME and WT for both parameters ($P = 0.02$ for A_E and $P < 0.001$ for A_D). There was no statistically significant difference in A_E and A_D between BCA and WT ($P = 0.61$ for A_E and $P = 0.12$ for A_D) and between BCA and ME ($P = 0.21$ for A_E and $P = 0.07$ for A_D). Fig. 1 shows schematic drawings of the enhancement pattern of the three tumor groups.

Table 1. General morphologic tumor characteristics on CT

	Basal cell adenoma	Myoepithelioma	Warthin tumor	*P*
No. of cases	19	12	23	
Size (cm), mean±SD	2.4±1.15 (0.9–4.3)	2.3±0.86 (1.1–3.6)	2.8±0.89 (1.8–4.5)	0.83
Location, n (%)				0.94
Superficial lobe	15 (78.9)	10 (83.3)	18 (78.3)	
Deep lobe	4 (21.1)	2 (16.7)	5 (21.7)	
Margin, n (%)				0.12
Well-defined	18 (94.7)	8 (66.7)	22 (95.7)	
Microlobulated	1 (5.3)	3 (25)	1 (4.3)	
Ill-defined	0 (0)	1 (8.3)	0 (0)	
Cystic change, n (%)				0.26
Yes	9 (47.4)	6 (50)	7 (30.4)	
No	10 (52.6)	6 (50)	16 (69.6)	
Calcification, n (%)				0.75
Yes	2 (10.5)	1 (8.3)	1 (4.3)	
No	17 (89.5)	11 (91.7)	22 (95.7)	

SD, standard deviation.

Table 2. Results of CT parameters

	Basal cell adenoma	Myoepithelioma	Warthin tumor	*P*
A_E	114.6±39.3 (33.3–173.5)	141.0±38.4 (67.6–187.1)	103.4±20.2 (68–154.6)	0.008
A_D	83.5±24.6 (21.9–139.1)	101.7±18.2 (76.3–128)	70.2±11.8 (45.4–90.6)	<0.001
A_{WO}	31.2±37.8 (-39.9 to 98.9)	39.3±35.8 (-20.7 to 89.9)	33.2±15.7 (11.5–81.6)	0.75
RPEWR	18.4±40.0 (-103.3 to 63.9)	22.5±24.9 (-25.9 to 50.7)	31.2±9.8 (16.1–52.8)	0.31

Data are presented as mean ± standard deviation with ranges in parentheses.
The *P* values are for comparisons among basal cell adenoma, myoepithelioma, and Warthin tumor by using the analysis of variance test.
A_E, attenuation value at early-phase CT; A_D, attenuation value at delayed-phase CT; A_{WO}, washout attenuation; RPEWR, relative percentage enhancement washout ratio.

Table 3. Comparison of CT parameters among groups

	Basal cell adenoma vs. myoepithelioma	Basal cell adenoma vs. Warthin tumor	Myoepithelioma vs. Warthin tumor
A_E	0.21	0.61	0.02
A_D	0.07	0.12	<0.001
A_{WO}	0.91	0.99	0.93
RPEWR	0.98	0.47	0.61

P values are for comparisons among basal cell adenoma, myoepithelioma, and Warthin tumor by using the post hoc Tukey test of the analysis of variance test ($P < 0.05$).
A_E, attenuation value at early-phase CT; A_D, attenuation value at delayed-phase CT; A_{WO}, washout attenuation; RPEWR, relative percentage enhancement washout ratio.

Most tumors in each group demonstrated a washout pattern of enhancement, as based on the results of A_{WO} and RPEWR (Figs. 2–4) and included 15 (79%) of 19 BCAs (79%), 9 of 12 MEs (75%), and 23 of 23 WTs (100%). The remaining four BCAs (21%) and three MEs (25%) showed a gradual enhancement pattern. As for A_{WO}, although ME showed the greater mean value (39.3±35.8) than BCA (31.2±37.8) and WT (33.2±15.7), there was no statistically significant difference among three tumor groups ($P = 0.75$). Likewise, although WT (31.2±9.8) showed the greater mean RPEWR value than ME (22.5±24.9) and BCA (18.4±40.0), no statistically significant difference was found among the three types of tumor ($P = 0.31$).

Discussion

BCAs and MEs are uncommon benign tumors of the salivary gland, both of which were accepted as a histologically distinct entity since 1991 by the World Health Organization. They comprise 1%–2% and 1.5% of all salivary gland epithelial tumors, respectively, and predominantly occur in the parotid gland (15–17, 19, 21). Histologically, BCAs are characterized by a monomorphic population of basaloid cells sharply delineated from the stroma by basement membrane. The lack of myxochondroid stroma, myoepithelial cells, and mesenchymal mucin within the tumors helps distinguish BCAs from PAs (15–17). Four histologic subtypes are recognized according to cellular growth patterns, including solid, tubular, trabecular, and membranous, with the solid subtype being the most frequent form and the membranous subtype having a high recurrence rate (14, 16, 21). In contrast, MEs are composed almost exclusively of sheets, islands, or cords of cells with myoepithelial differentiation with spindle, plasmacytoid, epithelioid, or clear cytoplasmic features (18, 19, 24). Surgical excision is the treatment of choice for both tumors.

In this study, both BCAs and MEs most frequently demonstrated rapid enhancement and a washout pattern on two-phase CT scans, which was reported to be characteristic of WTs (2, 13). Based on the results of A_{WO} and RPEWR in our series, BCAs, MEs, and WTs showed a washout pattern of enhancement in 79%, 75%, and 100%, respectively. Compared to A_{WO} which simply represents the difference of the attenuation values between A_E and A_D, the RPEWR is more objective, in that it represents the

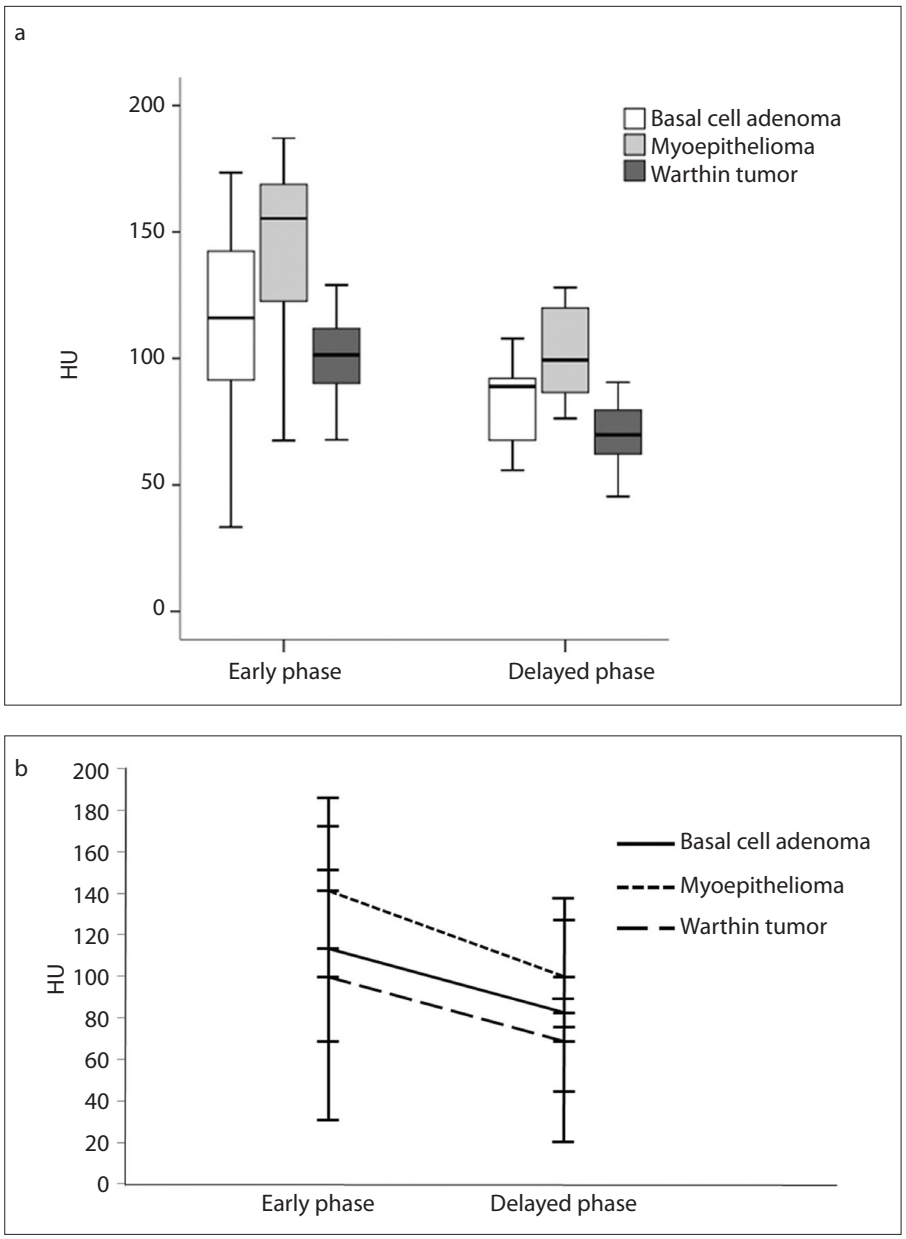

Figure 1. a, b. Boxplot **(a)** shows the distribution of the attenuation values of the solid component of the tumors at early and delayed phases. The thick horizontal line is the median (50th percentile) of the measured attenuation values, and the tops and bottoms of the boxes represent the 25th and 75th percentiles, respectively. Whiskers represent the range from the largest to smallest observed data sets within the 1.5 interquartile range presented by the box. Graph **(b)** shows the lines connecting mean attenuation values between the early and delayed phases on two-phase CT; washout pattern of enhancement is clearly shown in all three tumor groups.

ratio of A_{WO} to A_E and is useful when the precontrast CT scans are not available (23). In this study, although both A_{WO} and RPEWR of MEs were greater than those of BCAs and WTs, the difference was not statistically significant between the tumors. Our study also showed that both A_E and A_D were greater for MEs than for BCAs and WTs with statistically significant difference only being noted between MEs and WTs for both parameters. Although we have no clear explanation, we presume that the different histologic constituents among the different tumors might partly account for it.

The washout enhancement pattern in these tumors might be attributed to hypercellularity and the small volume of stroma as previously shown in the studies using dynamic CT and MRI (3, 25). The washout of contrast material depends on the difference in the amount of contrast material within the tumor between the intravascular and extravascular phases. Tumors with low cellularity and large extracellular space have a tendency to retain contrast material, resulting in a low washout ratio. In contrast, tumors with high cellularity and small extracellular space retain less contrast material, resulting in a high washout ratio (3). On dynamic contrast-enhanced MRI, this washout pattern at two-phase CT, as seen in tumors with small extracellular space such as malignant lymphoma, can be a correlate to small Ve, the extravascular extracellular space volume fraction (26).

Previous reports with multiple imaging modalities have attempted to correlate the imaging characteristics of the salivary gland tumors with the histopathologic features. In their study on CT-histopathologic correlation for WTs, Woo et al. (13) reported that WTs had densely packed, capillary-like vessel networks with a high vascularity, which was presumed to be responsible for the cause of rapid contrast enhancement at early phase on two-phase CT scans. This correlates with a high microvessel count in the study by Yabuuchi et al. (3). Woo et al. (13) also reported that leaky blood vessels accounted for early washout of contrast material on two-phase CT scans. Similar to WTs, solid type BCAs were reported to have numerous endothelial-lined vascular channels with prominent small capillaries and venules (14, 16, 17, 21), accounting for early enhancement with subsequent washout (6, 21, 22). Likewise, MEs were reported to demonstrate epithelial nets with numerous blood vessels on histologic examination (18, 24). In their study with 10 MEs of the parotid gland, Wang et al. (18) reported that all tumors appeared as homogeneous or heterogeneous well enhancing nodules on postcontrast CT scans obtained at 40 s after the onset of contrast injection. Although the features of MEs on dynamic CT and MRI have seldom been reported, one case of ME included in the study by Yabuuchi et al. (3) demonstrated early enhancement and high washout on dynamic contrast-enhanced MRI, similar to WTs.

Although the majority of BCAs and MEs demonstrated the washout enhancement pattern in this study, a small portion of BCAs (4/19, 21%) and MEs (3/12, 25%) showed gradual enhancement pattern on two-phase CT scans. The enhancement pattern other than the washout pattern has also been reported in cases of BCA and ME. As for BCAs, Lee et al. (21) reported that while the solid type showed early strong

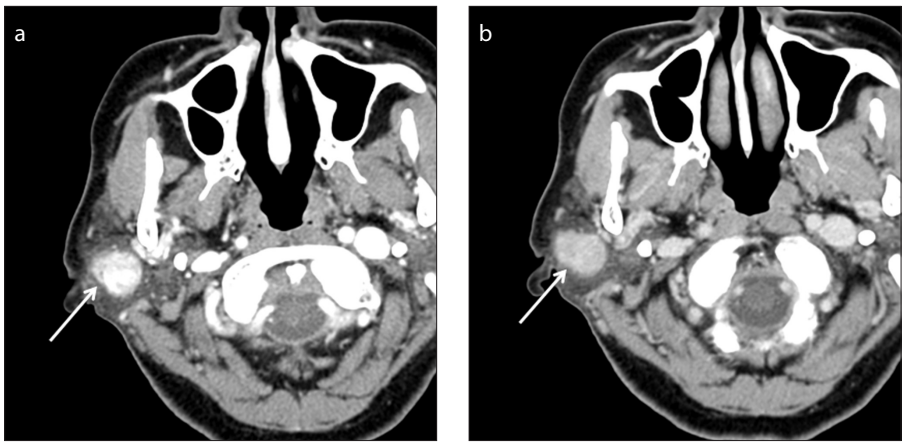

Figure 2. a, b. Basal cell adenoma of the right parotid gland in a 71-year-old woman. A well-defined ovoid mass *(arrow)* is located in the superficial lobe of the right parotid gland on two-phase CT scans. The mass shows marked contrast enhancement at early phase **(a)** and homogeneous washout of contrast material at delayed phase **(b)**. The measured A_E and A_D are 116 and 87.7, respectively, resulting in A_{WO} of 28.3 and RPEWR of 24.4%.

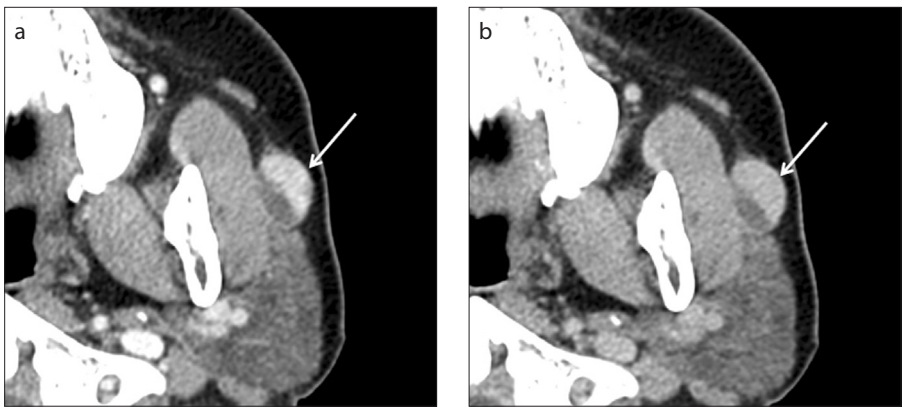

Figure 3. a, b. Myoepithelioma of the left parotid gland in a 49-year-old woman. A well-defined ovoid mass *(arrows)* is seen in the superficial lobe of the left parotid gland on two-phase CT scans. The mass is composed of a large solid component laterally and a smaller cystic component medially, the latter of which demonstrates marked homogeneous contrast enhancement at early phase **(a)** and homogeneous washout of contrast material at delayed phase **(b)**. The measured A_E and A_D of the solid component of the tumor are 122.6 and 96.3, respectively, resulting in A_{WO} of 26.3 and RPEWR of 21.5%.

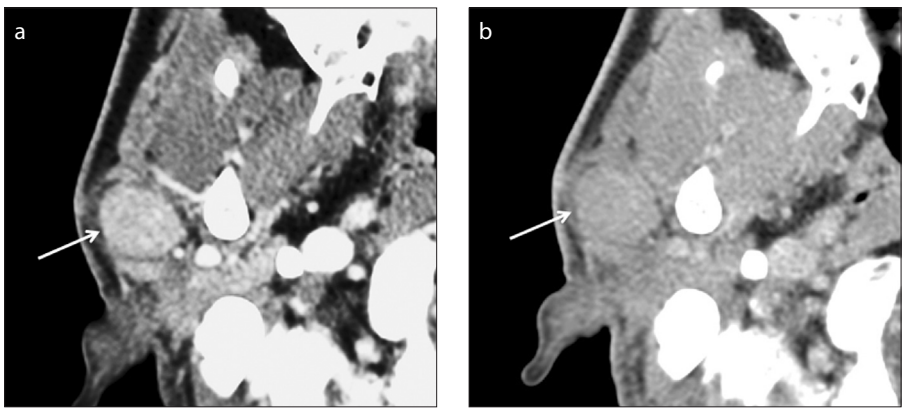

Figure 4. a, b. Warthin tumor of the right parotid gland in a 50-year-old man. A well-defined ovoid mass *(arrow)* is seen in the superficial lobe of the right parotid gland on two-phase CT scans. The mass shows marked homogeneous contrast enhancement at early phase **(a)** and homogeneous washout of contrast material at delayed phase **(b)**. The measured A_E and A_D are 121 and 90, respectively, resulting in A_{WO} of 31 and RPEWR of 25.6%.

enhancement and a washout pattern like WTs, the tubular/trabecular type demonstrated less strong early enhancement and the gradual enhancement pattern on two-phase CT scans, as seen in PAs. In their two-phase CT study by Joo et al. (20), all of six BCAs showed increased enhancement on delayed phase CT scans. The various pattern of enhancement reported in the different studies might be ascribed to histologic variations that consist of the individual tumor. Likewise, MEs might also demonstrate the gradual enhancement pattern, if they contain a large area of collagenous or mucoid stroma (18, 24). Joo et al. (20) reported that while only one of three MEs showed decreased enhancement, the remaining two MEs showed increased enhancement on delayed phase CT scans. In their study with contrast-enhanced MRI, Ding et al. (19) reported that all five MEs exhibited early moderate to marked enhancement on the axial images, followed by prolonged enhancement on the consecutive coronal images. Their results are apparently in contrast to ours. The difference in the results might be related to the concept of prolonged enhancement used in their study. They neither defined the term clearly nor provided the numeric data of the degree of enhancement objectively. Through the figures in their article, we presume that they might have used prolonged enhancement when the tumor demonstrated enhancement at delayed phase, irrespective of washout or gradual enhancement pattern.

The clinical implications of this study may not be great, because the treatment would not be changed, no matter what diagnoses are made. In general, identification of the histology of various benign tumors on preoperative imaging studies would be less important than differentiation between benign and malignant tumors. However, from the radiologist's standpoint, every trial should be done to recognize the histologic nature of the lesions during imaging evaluation, because the biologic behavior, such as malignant potential and propensity to recur, may be different among the various benign tumors. For example, the malignant potential has been estimated as 9.5% of PAs after 15 years, less than 1% of WTs, about 4% of BCAs, and up to 10% of MEs (8, 15, 18, 27).

Radiation exposure is an important issue of two-phase CT, which inevitably delivers a greater amount of radiation, compared with conventional single-phase CT. In

the present study, the measured CTDIvol ranged from 10.9 to 37.52 mGy per phase, which was comparable to the reported CTDIvol in neck volume CT (2, 3). The scheme to reduce the radiation dose such as automatic tube current modulation technique is always recommended during two-phase CT (28).

This study had several limitations. First, we did not perform the radiologic-pathologic correlation of the individual tumor, which might have explained the differences of the attenuation characteristics among tumors, such as A_E and A_D. Second, among the various types of benign parotid tumors, we only selected BCAs and MEs to compare their enhancement pattern with that of WTs. Other less common benign tumors such as oncocytomas may manifest as a mass with the same enhancement pattern as WTs. We expect further validation with a large cohort of various benign tumors. Third, we did not obtain precontrast CT scans which are essential to know the actual increment of the attenuation values on postcontrast CT scans. This inevitably hindered us from analyzing the full range of enhancement pattern of the tumors on two-phase CT scans.

In conclusion, BCAs and MEs of the parotid gland demonstrated early enhancement and a washout pattern on two-phase CT scans, which is regarded as the characteristic features of WTs. The pattern of enhancement seen in these tumors seems to reflect the prominent vasculature within the solid component of the tumors histologically. We suggest that in addition to WTs, BCAs and MEs might be included in the list of differential diagnosis, when the parotid tumors show early enhancement and a washout pattern on two-phase CT scans.

Conflict of interest disclosure

The authors declared no conflicts of interest.

References

1. Zhan KY, Khaja SF, Flack AB, Day TA. Benign parotid tumors. Otolaryngol Clin North Am 2016; 49:327–342. [CrossRef]
2. Choi DS, Na DG, Byun HS, et al. Salivary gland tumors: evaluation with two-phase helical CT. Radiology 2000; 214:231–236. [CrossRef]
3. Yabuuchi H, Fukuya T, Tajima T, Hachitanda Y, Tomita K, Koga M. Salivary gland tumors: diagnostic value of gadolinium-enhanced dynamic MR imaging with histopathologic correlation. Radiology 2003; 226:345–354. [CrossRef]
4. Okahara M, Kiyosue H, Hori Y, Matsumoto A, Mori H, Yokoyama S. Parotid tumors: MR imaging with pathological correlation. Eur Radiol 2003; 13(Suppl 4):L25–33. [CrossRef]
5. Eida S, Sumi M, Sakihama N, Takahashi H, Nakamura T. Apparent diffusion coefficient mapping of salivary gland tumors: prediction of the benignancy and malignancy. Am J Neuroradiol 2007; 28:116–121.
6. Yerli H, Aydin E, Coskun M, et al. Dynamic multislice computed tomography findings for parotid gland tumors. J Comp Assist Tomogr 2007; 31:309–316. [CrossRef]
7. Alibek S, Zenk J, Bozzato A, et al. The value of dynamic MRI studies in parotid tumors. Acad Radiol 2007; 14:701–710. [CrossRef]
8. Yabuuchi H, Matsuo Y, Kamitani T, et al. Parotid gland tumors: can addition of diffusion-weighted MR imaging to dynamic contrast-enhanced MR imaging improve diagnostic accuracy in characterization? Radiology 2008; 249:909–916. [CrossRef]
9. Eida S, Sumi M, Nakamura T. Multiparametric magnetic resonance imaging for the differentiation between benign and malignant salivary gland tumors. J Magn Reson Imaging 2010; 31:673–679. [CrossRef]
10. Jin GQ, Su DK, Xie D, Zhao W, Liu LD, Zhu XN. Distinguishing benign from malignant parotid gland tumours: low-dose multi-phasic CT protocol with 5-minute delay. Eur Radiol 2011; 21:1692–1698. [CrossRef]
11. Sumi M, Van Cauteren M, Sumi T, Obara M, Ichikawa Y, Nakamura T. Salivary gland tumors: use of intravoxel incoherent motion MR imaging for assessment of diffusion and perfusion for the differentiation of benign from malignant tumors. Radiology 2012; 263:770–777. [CrossRef]
12. Sumi M, Nakamura T. Head and neck tumours: combined MRI assessment based on IVIM and TIC analyses for the differentiation of tumors of different histological types. Eur Radiol 2014; 24:223–231. [CrossRef]
13. Woo SH, Choi DS, Kim JP, et al. Two-phase computed tomography study of Warthin tumor of parotid gland: differentiation from other parotid gland tumors and its pathologic explanation. J Comp Assist Tomogr 2013; 37:518–524. [CrossRef]
14. Jang M, Park D, Lee SR, et al. Basal cell adenoma in the parotid gland: CT and MR findings. Am J Neuroradiol 2004; 25:631–635.
15. Chawla AJ, Tan TY, Tan GJ. Basal cell adenomas of the parotid gland: CT scan features. Eur J Radiol 2006; 58:260–265. [CrossRef]
16. Okahara M, Kiyosue H, Matsumoto A, et al. Basal cell adenoma of the parotid gland: MR imaging findings with pathological correlation. Am J Neuroradiol 2006; 27:700–704.
17. Shi L, Wang YX, Yu C, Zhao F, Kuang PD, Shao GL. CT and ultrasound features of basal cell adenoma of the parotid gland: a report of 22 cases with pathologic correlation. Am J Neuroradiol 2012; 33:434–438. [CrossRef]
18. Wang S, Shi H, Wang L, Yu Q. Myoepithelioma of the parotid gland: CT imaging findings. Am J Neuroradiol 2008; 29:1372–1375. [CrossRef]
19. Ding J, Wang W, Peng W, Zhou X, Chen T. MRI and CT imaging characteristics of myoepithelioma of the parotid gland. Acta Radiol 2016; 57:837–843. [CrossRef]
20. Joo YH, Kim JP, Park JJ, Woo SH. Two-phase helical computed tomography study of salivary gland warthin tumors: a radiologic findings and surgical applications. Clin Exp Otorhinolaryngol 2014;7:216–221. [CrossRef]
21. Lee DK, Chung KW, Baek CH, Jeong HS, Ko YH, Son YI. Basal cell adenoma of the parotid gland: characteristics of two-phase helical computed tomography and magnetic resonance imaging. J Comp Assist Tomogr 2005; 29:884–888. [CrossRef]
22. Yerli H, Teksam M, Aydin E, Coskun M, Ozdemir H, Agildere AM. Basal cell adenoma of the parotid gland: dynamic CT and MRI findings. Br J Radiol 2005; 78:642–645. [CrossRef]
23. Kamiyama T, Fukukura Y, Yoneyama T, Takumi K, Nakajo M. Distinguishing adrenal adenomas from nonadenomas: combined use of diagnostic parameters of unenhanced and short 5-minute dynamic enhanced CT protocol. Radiology 2009; 250:474–481. [CrossRef]
24. Sciubba JJ, Brannon RB. Myoepithelioma of salivary glands: report of 23 cases. Cancer 1982; 49:562–572. [CrossRef]
25. Bisdas S, Baghi M, Wagenblast J, et al. Differentiation of benign and malignant parotid tumors using deconvolution-based perfusion CT imaging: feasibility of the method and initial results. Eur J Radiol 2007; 64:258–265. [CrossRef]
26. Kitamoto E, Chikui T, Kawano S, et al. The application of dynamic contrast-enhanced MRI and diffusion-weighted MRI in patients with maxillofacial tumors. Acad Radiol 2015; 22:210–216. [CrossRef]
27. Seifert G, Sobin LH. The World Health Organization's histological classification of salivary gland tumors. a commentary on the second edition. Cancer 1992; 70:379–385. [CrossRef]
28. Russell MT, Fink JR, Rebeles F, Kanal K, Ramos M, Anzai Y. Balancing radiation dose and image quality: clinical applications of neck volume CT. Am J Neuroradiol 2008; 29:727–731. [CrossRef]